UNCECOMP 2015
1st ECCOMAS Thematic Conference on
International Conference on Uncertainty Quantification in
Computational Sciences and Engineering
M. Papadrakakis, V. Papadopoulos, G. Stefanou (eds.)
Crete Island, Greece, 25–27 May 2015

MODELING OF UNCERTAIN SPECTRA THROUGH STOCHASTIC AUTOREGRESSIVE SYSTEMS

Yiwei Wang[1], X.Q. Wang[1], Marc P. Mignolet[1], Shuchi Yang[2], and P.C. Chen[2]

[1] SEMTE Faculties of Mechanical and Aerospace Engineering
Arizona State University, Tempe, AZ 85287, USA
e-mail: yiwei.wang.3@asu.edu, xiaoquan.wang.1@asu.edu, marc.mignolet@asu.edu

[2] ZONA Technology
9489 E. Ironwood Square Drive, Scottsdale, AZ 85258-4578, USA
shuchi@zonatech.com, pc@zonatech.com

Keywords: Uncertain Power Spectral Densities, Stochastic Autoregressive Models, Maximum Entropy, Random Matrices, Maximum Likelihood Identification.

Abstract. *The focus of this investigation is on the formulation and validation of a modeling strategy of the uncertainty that may exist on the specification of the power spectral density of scalar stationary processes and on the spectral matrices of vector ones. These processes may, for example, be forces on a structure originating from natural phenomena which are coarsely modeled (i.e., with epistemic uncertainty) or are specified by parameters unknown (i.e., with aleatoric uncertainty) in the application considered. The propagation of the uncertainty, e.g., to the response of the structure, may be carried out provided that a stochastic model of the uncertainty in the power spectral density/matrix is available from which admissible samples can be efficiently generated. Such a stochastic model will be developed here through an autoregressive-based parameterization of the specified baseline power spectral density/matrix and of its random samples. Autoregressive (AR) models are particularly well suited for this parametrization since their spectra are known to converge to a broad class of spectra (all non-pathological spectra) as the AR order increases. Note that the characterization of these models is not achieved directly in terms of their coefficients but rather in terms of their reflection coefficients which lie (or their eigenvalues in the vector process case) in the domain [0,1) as a necessary and sufficient condition for stability. Maximum entropy concepts are then employed to formulate the distribution of the reflection coefficients in both scalar and vector process case leading to a small set of hyperparameters of the uncertain model. Depending on the information available, these hyperparameters could either be varied in a parametric study format to assess the effects of uncertainty or could be identified, e.g., in a maximum likelihood format, from observed data. The validation and assessment of these concepts is finally achieved on the response of an uncertain 4-degree of freedom system subjected to white noise and on the response of an F-15 aircraft to random buffeting loads.*

1 INTRODUCTION

While generally considered deterministic, the power spectral density of a stationary process may in fact exhibit randomness that results from uncertainty on the underlying conditions under which the process develops. For example, accepted models of spectra of physical processes such as ocean waves, ground motions, wind forces, etc. often depend on parameters such as depth of the ocean, composition of the ground at the location on earth considered, etc. Uncertainty on the exact values of these parameters thus creates a similar uncertainty on the spectra. Another potential source of uncertainty, i.e., epistemic, also lies in the differences between accepted model and actual spectra.

If the process being modeled is the input to a system, e.g., the excitation on a structure, the uncertainty on its spectral description propagates to the output or response the uncertainty of which then needs to be assessed. This task requires the availability of a modeling strategy of the uncertainty in the input process spectra which:

(a) is physically/mathematically acceptable, i.e., no power spectral matrix sample should exhibit negative or zero power, nor should it lead to infinite values which would be indicative of a persistent nonstationarity,

(b) is flexible to match any specified “baseline model” (corresponding to a zero level of uncertainty),

(c) involves parameters that can be identified from data,

(d) has a tunable complexity to adapt to situations where little information is available (likely often) but also when more experimental data is known, and

(e) is applicable to both power spectra of scalar processes and spectral matrices of vector ones.

Certainly, a random spectrum could be viewed as a stochastic process indexed by frequency. However, this process would have to be positive (thus non-Gaussian) and could not be stationary owing to the decay of physical spectra at high frequencies, thereby preventing straightforward modeling options. An alternate strategy is adopted here which relies on a parametrized representation of the power spectral densities/matrices of both baseline and random samples. Then, the introduction of uncertainty in the power spectral density/matrix will be accomplished through the randomization of the parameters. The key questions arising then are:

(i) what parametrized form of the spectrum should be adopted

(ii) what is the distribution of the parameters of this model

which should both be addressed within the constraints (a)-(e) above.

With regard to question (i), it is proposed here to parametrize the power spectral density/matrix through the autoregressive (AR) modeling technique [1] which is particularly well suited since AR spectra are known to converge to any non-pathological physical spectrum as the AR order increases (see for example [2] for discussion). While stochastic AR models have been investigated in the past, e.g., see [3-7], they do not appear to have been considered for a priori modeling as is intended here and have very seldom addressed the vector process case.

For completeness, the following section briefly reviews the definition, construction, and properties of AR models before the issue of distribution of parameters, i.e., issue (ii) above, is considered in the ensuing section. A series of applications are then considered to validate the methodology.

2 AUTOREGRESSIVE MODELING

2.1 Definition and Yule-Walker Equations

A discrete stationary random vector process **y** is referred to as an autoregressive process of order *m* if its samples $\mathbf{y}_n$ are related by the recursion

$$\mathbf{y}_n = -\sum_{k=1}^{m} \hat{A}_k \; \mathbf{y}_{n-k} + \hat{B}_0 \; \hat{\mathbf{w}}_n \tag{1}$$

where $\hat{A}_k$ and $\hat{B}_0$ are constant *N*x*N* matrices, *N* being the number of components of **y**, and $\hat{\mathbf{w}}$ is a discrete white noise vector process with covariance matrix equal to the identify matrix I_N. The matrices $\hat{A}_k$ and $\hat{B}_0$ and the autocorrelation matrices

$$R_{\mathbf{yy}}(p) = E\left[\mathbf{y}_n \, \mathbf{y}_{n+p}^T\right] \tag{2}$$

where $E[\cdot]$ denotes the expected value operation and ^{T} is the operator of vector/matrix transposition, are related by the Yule-Walker equations [1]

$$R_{\mathbf{yy}}(-p) + \sum_{k=1}^{m} \hat{A}_k \; R_{\mathbf{yy}}(k-p) = 0 \text{ for } p = 1, 2, \ldots \tag{3}$$

and

$$R_{\mathbf{yy}}(0) + \sum_{k=1}^{m} \hat{A}_k \; R_{\mathbf{yy}}(k) = \hat{B}_0 \; \hat{B}_0^T \tag{4}$$

where it is noted that

$$R_{\mathbf{yy}}(-p) = \left[R_{\mathbf{yy}}(p)\right]^T . \tag{5}$$

Recognizing Eq. (1) as a filtering of the white noise process $\hat{\mathbf{w}}$, it is readily concluded that the spectral matrix $S_{\mathbf{yy}}(\omega)$ of the vector process **y** can be directly evaluated from the matrices $\hat{A}_k$ and $\hat{B}_0$ as

$$S_{\mathbf{yy}}(\omega) = \frac{1}{2\,\omega_c}\left[I + \sum_{k=1}^{m} \hat{A}_k \, e^{i\,k\,\omega\,\Delta t}\right]^{-1} \hat{B}_0 \; \hat{B}_0^T \left[I + \sum_{k=1}^{m} \hat{A}_k \, e^{-i\,k\,\omega\,\Delta t}\right]^{-T} . \tag{6}$$

where Δt denotes the sampling time and $\omega_c = \pi / \Delta t$ the corresponding Nyquist frequency.

Equations (3), (4), and (6) are the basis for the autoregressive spectral modeling approach. Specifically, given the autocorrelation matrices $R_{\mathbf{yy}}(p)$, *p* = 0, 1, .., *m*, the Yule-Walker equations (3) are first solved to yield the matrices $\hat{A}_k$. This is easily accomplished as these equations are linear in those matrices. Next, the matrix $\hat{B}_0 \; \hat{B}_0^T$ is determined from Eq. (4) and finally, the AR spectral matrix can be evaluated at any frequency $\omega \in [-\omega_c, \omega_c]$ from Eq. (6). The autocorrelation matrices $R_{\mathbf{yy}}(p)$ which are the start of the above computations can either be obtained from a particular target spectral matrix $S_T(\omega)$ as

$$R_{\mathbf{yy}}(p) = \int_{-\omega_c}^{\omega_c} S_T(\omega)\, e^{i\,p\,\omega\,\Delta t}\, d\omega \tag{7}$$

or be estimated from the time history $\mathbf{y}_n$, *n* = 1, ..., *M*, as

$$R_{\mathbf{yy}}(p) = \frac{1}{M-p} \sum_{n=1}^{M-p} \mathbf{y}_n \, \mathbf{y}_{n+p}^T \,. \tag{8}$$

When proceeding from a target spectral matrix, Eq. (7), it can be shown, see discussion of [2] and references therein, that

$$S_{\mathbf{yy}}(\omega) \to S_T(\omega) \quad \text{as} \quad m \to \infty \tag{9}$$

unless $S_T(\omega)$ is a pathological spectral matrix satisfying

$$\int_{-\omega_c}^{\omega_c} \mathrm{tr}\{\log[S_T(\omega)]\}\, d\omega = -\infty \tag{10}$$

where $\mathrm{tr}\{A\}$ is the trace of an arbitrary matrix *A*. The convergence property of Eq. (9) demonstrates that autoregressive models are appropriate parametrizations of any non-pathological power spectral matrix and thus can be used to represent both the specified baseline power spectral matrix and its uncertain samples.

The autoregressive models derived from the Yule-Walker equations (3) and (4) also possess the important property that the recursive computations of their samples according to Eq. (1) is stable [1]. This property can equivalently be stated in terms of the poles z_l of the transfer function of the autoregressive systems, i.e., the complex numbers *z* satisfying

$$\det\left[I + \sum_{k=1}^{m} \hat{A}_k \, z^{-k} \right] = 0 \,. \tag{11}$$

Specifically, stability implies that the poles are all of magnitude less than 1, $|z_l| < 1$.

2.2 Recursive Identification of the AR parameters

A completely equivalent approach to solving the Yule-Walker equations (3) and (4) for a particular value *m* of the order is to recursively determine all autoregressive models of orders 1 through *m* relying on the Levinson-Durbin (in the scalar process case) or Wiggins-Robinson (in the vector process case) algorithms, see [1,7,8]. Besides their computational advantages, these algorithms provide an important perspective on the origin of the stability property stated above.

To observe this connection, consider first the scalar process case and denote by $\hat{A}_k^{(p)}$ the autoregressive coefficient *k* for an autoregressive order *p*. Then, the Levinson-Durbin algorithm proceeds as follows:

$$\hat{A}_k^{(p+1)} = \hat{A}_k^{(p)} + \rho_p \, \hat{A}_{p-k+1}^{(p)}, \; k = 1, \ldots, p \tag{12}$$

and

$$\hat{A}_{p+1}^{(p+1)} = \rho_p \tag{13}$$

for p = 1, 2, ..., m-1. In these equations, ρ_p denote the reflection coefficients which can be computed [1] from the autocorrelation sequence $R_{\mathbf{yy}}(p)$ as

$$\rho_p = -\frac{\alpha_p}{V_p} \tag{14}$$

where

$$\alpha_p = R_{\mathbf{yy}}(p+1) + \sum_{k=1}^{p} \hat{A}_k^{(p)}\, R_{\mathbf{yy}}(p+1-k) \quad \text{and} \quad V_p = V_{p-1} + \rho_{p-1}\,\alpha_{p-1}. \quad (15),(16)$$

The recursion of Eqs (12) and (16) are initiated with the conditions

$$\rho_0 = \hat{A}_1^{(1)} = -R_{\mathbf{yy}}(1)/R_{\mathbf{yy}}(0) \quad \text{and} \quad V_1 = \left\{ \left[R_{\mathbf{yy}}(0)\right]^2 - \left[R_{\mathbf{yy}}(1)\right]^2 \right\} / R_{\mathbf{yy}}(0). \quad (17),(18)$$

The reflection coefficients are important parameters that are revealed in the above algorithm. In fact, one of their key properties is that [1]

$-1 < \rho_p < 1$, p = 0, 1, ..., m-1 are necessary and sufficient conditions for the autoregressive system to be stable, i.e., $|z_l| < 1$ (19)

The extension of Eqs (12)-(18) to the case of vector autoregressive models has been carried out, e.g., [1,7,8] and proceeds from the autocorrelations sequence $R_{\mathbf{yy}}(p)$ with the following recursive evaluation of the associated matrices $\hat{C}_k^{(p)}$ and $\hat{D}_k^{(p)}$ yielding the desired auto-regressive coefficient matrices $\hat{A}_k^{(p)}$.

(i) For a particular order p, compute first the matrix K_p

$$K_p = \sum_{k=0}^{p} \hat{C}_k^{(p)} R_{\mathbf{yy}}(p+1-k) \left[\hat{C}_0^{(0)}\right]^T \quad (20)$$

(ii) Construct by Cholesky decomposition the lower triangular matrices P_p and Q_p such that

$$P_p^{-1} P_p^{-T} = I_N - K_p K_p^T \quad \text{and} \quad Q_p^{-1} Q_p^{-T} = I_N - K_p^T K_p \quad (21)$$

(iii) Determine the matrices $\hat{C}_k^{(p+1)}$ and $\hat{D}_k^{(p+1)}$ as

$$\hat{C}_k^{(p+1)} = P_p \left[\hat{C}_k^{(p)} - K_p\, \hat{D}_{p+1-k}^{(p)}\right] \quad \text{and} \quad \hat{D}_k^{(p+1)} = Q_p \left[\hat{D}_k^{(p)} - K_p^T\, \hat{C}_{p+1-k}^{(p)}\right] k = 1, ..., p \quad (22)$$

$$\hat{C}_{p+1}^{(p+1)} = -P_p \left[K_p\, \hat{D}_0^{(p)}\right] \quad \text{and} \quad \hat{D}_{p+1}^{(p+1)} = -Q_p \left[K_p^T\, \hat{C}_0^{(p)}\right] \quad (23)$$

$$\hat{C}_0^{(p+1)} = P_p\, \hat{C}_0^{(p)} \quad \text{and} \quad \hat{D}_0^{(p+1)} = Q_p\, \hat{D}_0^{(p)}. \quad (24)$$

The recursion is initiated at order p = 0 with $\hat{C}_0^{(0)} = \hat{D}_0^{(0)}$ lower triangular matrices such that

$$\left[\hat{C}_0^{(0)}\right]^{-1} \left[\hat{C}_0^{(0)}\right]^{-T} = R_{\mathbf{yy}}(0). \quad (25)$$

The process is completed by the evaluation of the autoregressive coefficient matrices $\hat{A}_k^{(m)}$ at order m as

$$\hat{A}_k^{(m)} = \left[\hat{C}_0^{(m)}\right]^{-1} \hat{C}_k^{(m)},\ k = 0, ..., m \quad \text{and} \quad \hat{B}_0^{(m)} = \left[\hat{C}_0^{(m)}\right]^{-1}. \quad (26)$$

The above equations demonstrate that the required information for the determination of the autoregressive model are the matrices $R_{\mathbf{yy}}(0)$ and K_p, p = 0, 1, ..., m-1 which have clear properties:

$$R_{\mathbf{yy}}(0) \text{ is symmetric positive definite} \tag{27}$$

and

$$K_p,\ p = 0, 1, ..., m\text{-}1, \text{ has eigenvalues only between -1 and +1 (not included)} \tag{28}$$

where the latter condition stems from Eq. (21). Further, as obtained in the scalar process case, the stability of the autoregressive model is guaranteed by the conditions (27) and (28) [1,8].

3 STOCHASTIC POWER SPECTRAL DENSITY/MATRIX MODELING

3.1 Overall Plan

As suggested in the Introduction, a stochastic modeling of the uncertainty in power spectral density/matrix will be carried out through an autoregressive parametrization. That is, the "baseline model", i.e., the power spectral density/matrix which would be imposed without uncertainty, will first be modeled as an autoregressive process of order high enough to achieve an appropriate match of the autoregressive approximation (see discussion in the Applications section). Then, the parameters of that model, denoted here as $\hat{\bar{A}}_k$ and $\hat{\bar{B}}_0$, will be randomized while keeping the autoregressive order constant to produce samples of the uncertain power spectral density/matrix through Eq. (6).

The distribution of the random AR matrices $\hat{A}_k$ and $\hat{B}_0$ should be carefully selected to (i) guarantee the stability of the stochastic AR models, which is required for the stationary of the underlying processes **y**, as well as (ii) satisfy the constraints (a)-(e) of the Introduction. Given that the stability is directly governed by the reflection coefficients as opposed to the parameters $\hat{A}_k$ and $\hat{B}_0$, the randomization will be performed directly on those coefficients and will maintain the required properties for stability. That is, in the scalar process case:

(P.1) model ρ_p, p = 0, 1, ..., m-1, as random variables defined strictly between -1 and +1 and $\hat{B}_0^2$ as a random strictly positive variable

while in the vector process case

(P.2) model K_p, p = 0, 1, ..., m-1, as random matrices with eigenvalues strictly between -1 and +1 and $R_{\mathbf{yy}}(0)$ as a symmetric positive definite matrix.

While the conditions defined in (P.1) and (P.2) are restrictive, they nevertheless leave a very broad ensemble of potential distributions which can be narrowed down by considering the constraints (b)-(e) of the Introduction. In that regard, it is proposed here to rely on the maximum entropy nonparametric methodology initially proposed in [9], see [10] for a recent review of its numerous applications and extensions. The fundamental problem addressed by this method is the modeling of random symmetric positive definite matrices, see next section for review, which is directly applicable to the variable $\hat{B}_0^2$ of the scalar problem and the matrix $R_{\mathbf{yy}}(0)$ of the vector one. It can further be applied, through appropriate transformations, to the modeling of the reflection coefficients ρ_p and matrices K_p.

Specifically, consider first the modeling of the random matrices K_p and denote their counterparts for the baseline model as $\overline{K}_p$. Then, express this matrix in its QR decomposition

$$\overline{K}_p = \overline{Q}_p \, \overline{R}_p \tag{29}$$

where $\overline{Q}_p$ are unitary matrices, i.e., satisfying $\overline{Q}_p \, \overline{Q}_p^T = I_N$, and $\overline{R}_p$ are symmetric positive definite matrices solution of

$$\overline{K}_p^T \, \overline{K}_p = \left[\overline{R}_p\right]^2 \tag{30}$$

In light of Eq. (28), $\overline{R}_p$ has eigenvalues in [0,1). Interestingly, the representation of random positive definite symmetric matrices with bounded eigenvalues has recently been studied either directly from the maximum entropy framework [11] or through a transformation [12] mapping it to another random positive definite matrix without bounds. The latter approach is adopted here because of its simplicity. In selecting the transformation, note that eigenvalues of $\overline{R}_p$ close to or equal to zero may occur but that eigenvalues equal to 1 are not admissible. These observations suggest that $\overline{R}_p$ could be expressed as

$$\overline{R}_p = \overline{U}_p \left[I_N + \overline{U}_p\right]^{-1} \quad \text{or} \quad \overline{U}_p = \left[I_N - \overline{R}_p\right]^{-1} - I_N . \tag{31), (32}$$

where $\overline{U}_p$ is positive definite without further bound constraint and thus can be modeled with the standard nonparametric approach. Following this approach, random matrices U_p are then generated from which random matrices R_p and K_p are obtained according to

$$R_p = U_p \left[I_N + U_p\right]^{-1} \tag{33}$$

and

$$K_p = \overline{Q}_p \, R_p = \overline{Q}_p \; U_p \left[I_N + U_p\right]^{-1}. \tag{34}$$

Note in Eq. (34) that the unitary matrix $\overline{Q}_p$ of the baseline model is used for the stochastic one as well, see [10].

The above procedure can also be applied in the scalar case to the reflection coefficients ρ_p, p = 0, 1, ..., m-1. For these scalar variables, the matrix $\overline{Q}_p$ simply reduces to ±1 according to the sign of the variable being modeled.

Consistently with maximum entropy concepts, and in the absence of any further information or requirement, it will be assumed here that all random variables/matrices are independent of each other.

3.2 Modeling of Random Positive Definite Matrices – The Maximum Entropy Based Nonparametric Method

The fundamental problem of the nonparametric approach is the simulation of random symmetric positive definite real matrices. Denote the random matrix to be simulated as A and assume that its mean is known as $\overline{A}$, i.e. $E[A] = \overline{A}$. Clearly, there is a broad set of statistical distributions of the elements A_{ij} of the matrix A that could be selected. Among those, it would be particularly desirable to select the one that places particular emphasis on “larger” deviations from the mean value, a desirable feature to assess, in a limited Monte Carlo study,

the robustness of a design to uncertainty. As discussed in [9,10], this property is achieved by the distribution of the elements A_{ij} that achieves the *maximum of the statistical entropy* under the stated constraints of symmetry, positive definiteness, known mean model, to which is added the nonsingularity of A to prevent the occurrence of zero eigenvalues if they are not physically expected in the problem. This maximum is satisfied (see [9,10]) when the matrices A are generated as

$$A = \overline{L}\, H\, H^T\, \overline{L}^T \tag{35}$$

where $\overline{L}$ is any decomposition, e.g., Cholesky, of $\overline{A}$ satisfying $\overline{A} = \overline{L}\,\overline{L}^T$. Further, H denotes a lower triangular random matrix the elements of which are all statistically independent of each other. Moreover, the probability density functions of the diagonal (H_{ii}) and off-diagonal elements (H_{il}) are

$$p_{H_{ii}}(h) = C_{ii}\, h^{p(i)} \exp\left[-\mu h^2\right] \ , \ h \geq 0 \tag{36}$$

and

$$p_{H_{il}}(h) = C_{il} \ \exp\left[-\mu h^2\right] \ , \ h \geq 0 \, , \ i \neq l \tag{37}$$

where

$$p(i) = N - i + 2\lambda - 1 \qquad \mu = \frac{N + 2\lambda - 1}{2} \tag{38),(39}$$

$$C_{ii} = \frac{2\mu^{[p(i)+1]/2}}{\Gamma\left(\left(p(i)+1\right)/2\right)} \qquad C_{il} = \sqrt{\frac{\mu}{\pi}} \tag{40),(41}$$

In these equations, N denotes the size of the matrices A and $\Gamma(.)$ denotes the Gamma function. In fact, it is readily seen that (see also Fig. 1)

(1) the off-diagonal elements H_{il}, $i \neq l$, are normally distributed (Gaussian) random variables with standard deviation $\sigma = 1/\sqrt{2\mu}$, and

(2) the diagonal elements H_{ii} are obtained as $H_{ii} = \sqrt{\frac{Y_{ii}}{\mu}}$ where Y_{ii} is Gamma distributed with parameter $\left(p(i)-1\right)/2$.

In the above equations, the parameter $\lambda > 0$ is the free parameter (hyperparameter) of the statistical distribution of the random matrices H and A and can be evaluated to meet any given information about their variability. For example, an overall measure of variability can be introduced as

$$\delta^2 = \frac{1}{N} E\left[\left\| H\, H^T - I_N \right\|_F^2\right] = \frac{N+1}{N + 2\lambda - 1} \tag{42}$$

where $\| \ \|_F$ denotes the Frobenius norm. The imposition of λ (e.g., through δ) coupled with Eqs (36)-(39), provides a complete scheme for the generation of random symmetric positive definite matrices A.

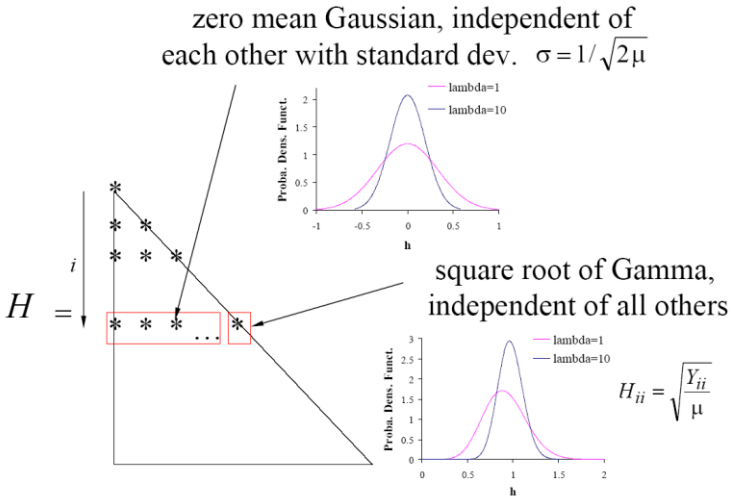

Figure 1: Structure of the random *H* matrices (figures for *n*=8, *i*=2, and λ=1 and 10).

3.3 Modeling Summary

The modeling process described in details above can be summarized as follows. The power spectral density/matrix provided (or determined) as "baseline model" is first approximated by an autoregressive spectra of order high enough to ensure an appropriate matching. This approximation is performed recursively with the Levinson-Durbin (scalar process) or Wiggins-Robinson (vector process) algorithms of Eqs (12)-(18) or (20)-(26), respectively. In this computation, the baseline reflection coefficients $\bar{\rho}_P$ or $\bar{K}_P$ are further processed to obtain the corresponding values/matrices $\bar{Q}_p$ and $\bar{R}_p$, see Eqs (29) and (30), and $\bar{U}_p$, see Eq. (32). These positive definite matrices are then decomposed in their Cholesky form, i.e., the lower triangular matrices $\bar{L}_p$ are determined which satisfy

$$\bar{U}_p = \bar{L}_p \, \bar{L}_p^T . \tag{43}$$

Moreover, a similar decomposition is performed for the baseline covariance matrix $\bar{R}_{\mathbf{yy}}(0)$, i.e.,

$$\bar{R}_{\mathbf{yy}}(0) = \bar{L}_R \, \bar{L}_R^T . \tag{44}$$

Next is the simulation phase in which the random variables/matrices are generated using the maximum entropy-base nonparametric approach. Specifically, considering the vector case, random lower triangular matrices H_R and H_p, p = 0, 1, ... m-1 are first simulated according to Eqs (36)-(41) and Fig. 1. Then, random covariance matrices $R_{\mathbf{yy}}(0)$ and random matrices U_p are obtained as

$$R_{\mathbf{yy}}(0) = \bar{L}_R \, H_R \, H_R^T \, \bar{L}_R^T \qquad \text{and} \qquad U_p = \bar{L}_p \, H_p \, H_p^T \, \bar{L}_p^T \quad . \tag{45),(46}$$

From the latter, random reflection coefficients K_P can be obtained from Eq. (34) and realizations of the stochastic autoregressive model can be determined through the recursive algorithm of Eq. (20)-(26).

The procedure is essentially similar in the scalar case with

$$\hat{B}_0^2 = \hat{\bar{B}}_0^2 \, H_R^2 \qquad \bar{\rho}_P = \mathrm{sgn}(\bar{\rho}_P)\frac{U_p}{1+U_p} \qquad (47), (48)$$

and with the marching of Eqs (12)-(18).

It should be noted that the use of the nonparametric methodology ensures the satisfaction of the requirements (b)-(d) stated in the Introduction. Clearly, the baseline model is included in Eqs (43)-(48). Further, as discussed in the previous section, the nonparametric approach only involves one hyperparameter, λ or δ, in its standard formulation of Eq. (36)-(41) but can refined (see [10,13]) to include as many as N. Finally, the identification of the hyperparameters from data can be achieved using standard methods, e.g., maximum likelihood, see [10] and example below.

4 APPLICATIONS AND VALIDATIONS

4.1 Scalar Case - Well Separated or Close Poles

This first example of application aims at highlighting the variability and interaction of the random poles of the stochastic autoregressive system when the baseline model exhibits either well separated or close poles. Two cases were analyzed both of which are order 4 models with $\hat{\bar{B}}_0 = 1$ and parameters $\hat{\bar{A}}_k$ consistent with imposed baseline model poles $\bar{z}_1, \bar{z}_1^*, \bar{z}_2, \bar{z}_2^*$ where * denotes the operation of complex conjugation.

In the first case, the poles $\bar{z}_1$ and $\bar{z}_2$ were selected to be well separated with one of them close to the unit circle and one away, i.e., $\bar{z}_1 = 0.98\, e^{i\pi/6}$ and $\bar{z}_2 = 0.5\, e^{i\pi/3}$. Then, shown in Fig. 2 are the locations of the poles of 100 samples of the corresponding stochastic AR model with $\delta = 0.3$. It is clearly seen that there is indeed no pole outside of the unit circle and thus all models are stable as expected. Further, the uncertainty has led to a rather uniform spread of the poles around $\bar{z}_2$ with changes in both radius and angle. However, the random poles around $\bar{z}_1$ are mostly spread in angle with limited variations in the radial direction as could be expected since they cannot cross the close by unit circle.

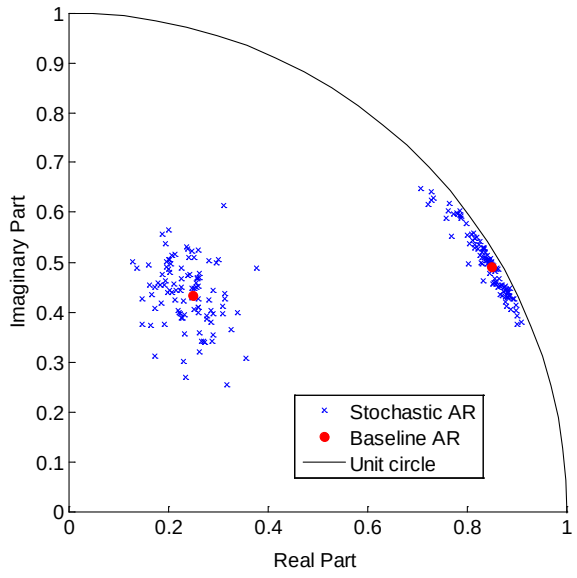

Figure 2: Location of poles of the baseline and stochastic AR models in the complex plane. Case 1.

The second case was designed to assess the interactions between poles close to each other and to the unit circle, at neighboring angles as could occur when the baseline spectrum model exhibits two close peaks. Specifically, the baseline poles were selected as $\bar{z}_1 = 0.98\ e^{i\pi/6}$ and $\bar{z}_2 = 0.98\ e^{i1.1\pi/6}$, i.e., close to the unit circle at 30 and 33 degrees. For small uncertainty levels, e.g., $\delta = 0.07$ in Fig. 3, the poles of the stochastic AR model form two distinct clusters, one around each baseline pole. When the uncertainty level is increased, see Fig. 4 for $\delta = 0.12$, the two clusters merge into a single one which includes both baseline poles. There is then significant variability on the frequencies at which peaks of the power spectral density will occur.

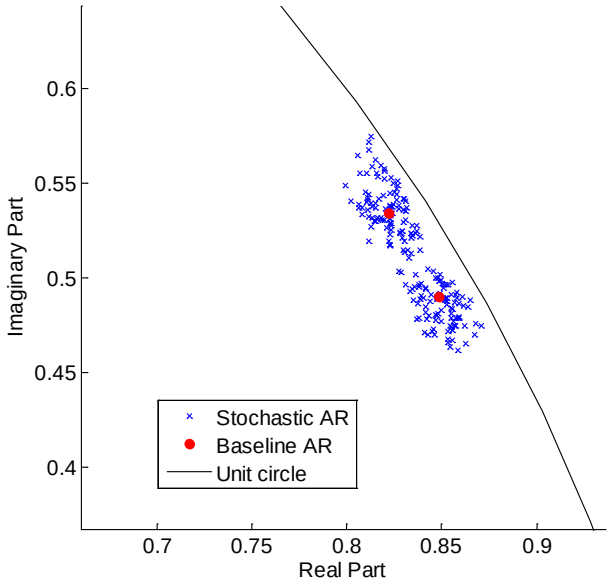

Figure 3: Location of poles of the baseline and stochastic AR models in the complex plane. Case 2. $\delta = 0.07$.

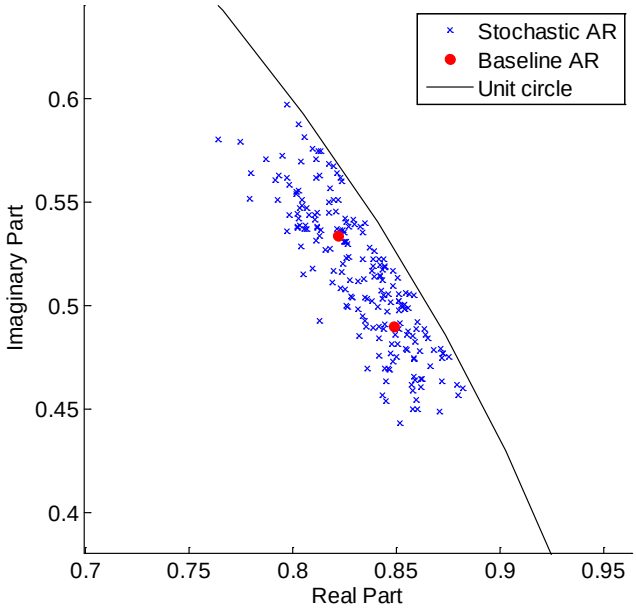

Figure 4: Location of poles of the baseline and stochastic AR models in the complex plane. Case 2. $\delta = 0.12$.

4.2 Scalar Case – A Structural Example

The response of the 4 degree of freedom system shown in Fig. 5 was considered for a first full validation of the autoregressive stochastic modeling approach. All springs were assumed to have the same stiffness k = 1N/m and a unit mass m = 1 kg was selected for all blocks. The damping was assumed to be classical with a 2% damping ratio on all modes. The system was subjected to the effects of a ground acceleration $a(t)$ white noise in the band $\omega \in [-\pi, \pi]$ rad/s and with power spectral density equal to 1 m^2/s^5.

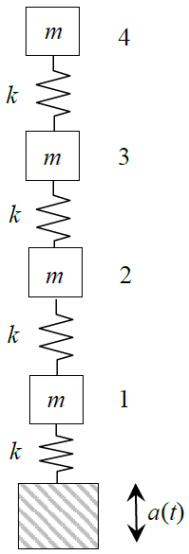

Figure 5: Four degree of freedom system subjected to ground motions.

Shown in Figs 6(a) and 7(a) are the power spectral densities of the displacements of the masses 1 and 2 as predicted directly from the equations of motion (curves "Displacements") which will serve as baseline models. Autoregressive approximations of these power spectral densities were first sought to establish the baseline values of the reflection coefficients. In selecting the order for these approximations, it should be recognized that the differences between the corresponding autoregressive power spectral densities (referred to as the "Baseline AR model") and their baseline counterparts are essentially epistemic uncertainties which can be absorbed in the overall uncertainty if they are small enough.

In light of this observation, the autoregressive order was selected as 15 and 25 for degree of freedoms 1 and 2, respectively. The need for the higher order for degree of freedom 2 results from the presence of a dip of the power spectral density (an antiresonance) at 1.4 rad/s; the convergence of the autoregressive model is known to be slower for power spectral densities with zeros/small values, see [2] and references therein. Small differences occur between the two sets of power spectral densities, the most significant ones being a slight difference on the frequency of mode 3 and the smoothing of the antiresonance both in Fig. 7(a). As expected, these differences can be reduced by increasing the autoregressive order.

These 2 baseline AR models were used to generate uncertain AR models with δ = 0.1 as described in the previous sections and 300 samples of each were simulated. The 5th and 95th percentiles of these power spectral densities were evaluated at each frequency independently and shown in green in Fig. 6(a) and 7(a) are the "bands of uncertainty" corresponding to the interval between these two percentiles. Note that the selected value of δ is larger than the epistemic uncertainty associated with the small differences between the baseline models (curves "Displacement") and their autoregressive approximations ("Baseline AR") as can be con-

firmed by comparing these differences to the width of the band. As a result, the baseline model curves are nearly completely within the uncertainty bands, with the exception of the neighborhood of the antiresonance. This issue should be of no concern given the very low energy levels of the antiresonance (note the log scale in Fig. 6(a) and 7(a)) but it could be resolved, if necessary, by simply increasing the autoregressive order until an appropriate capture of the antiresonance is achieved.

To complete the validation, shown in Figs 6(b) and 7(b) are the poles of the baseline and stochastic AR models which exhibit the features already observed in Figs (2)-(4), i.e., the clustering of the poles of the stochastic AR model around those of its baseline counterpart.

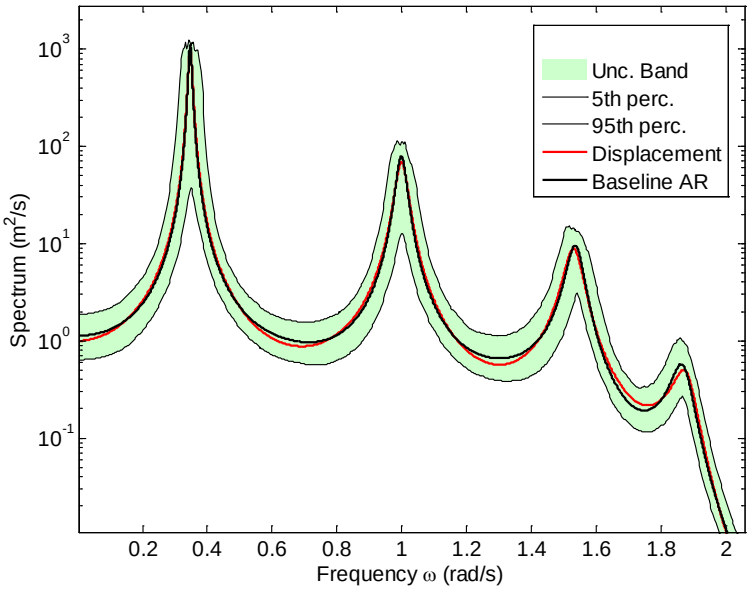

(a)

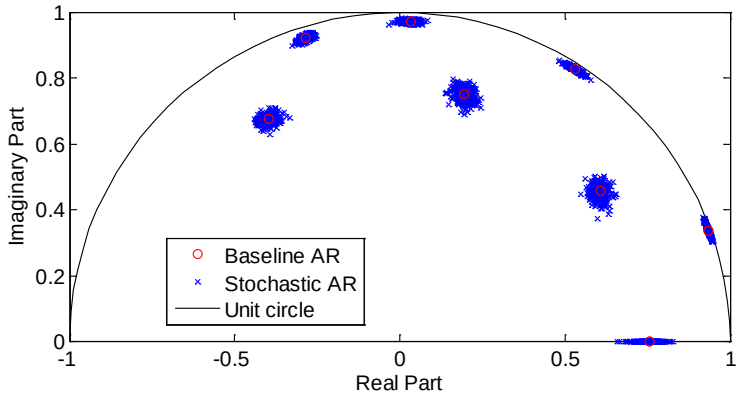

(b)

Figure 6: Analysis for degree of freedom 1. (a) Power spectral densities of the baseline model ("Displacement"), its autoregressive approximation ("Baseline AR"), and the 5th-95th percentile of the band of uncertainty of the stochastic model (in green). (b) Location of poles of the baseline and stochastic AR models in the complex plane. $\delta = 0.1$.

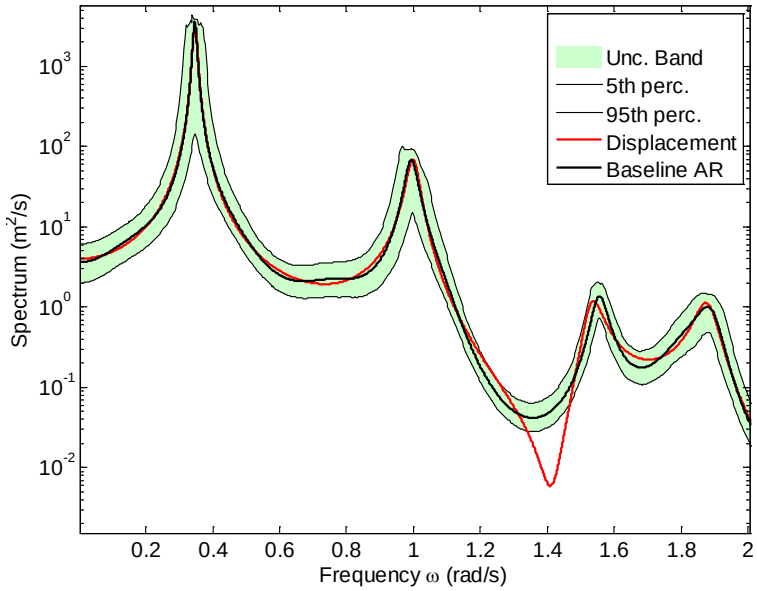

(a)

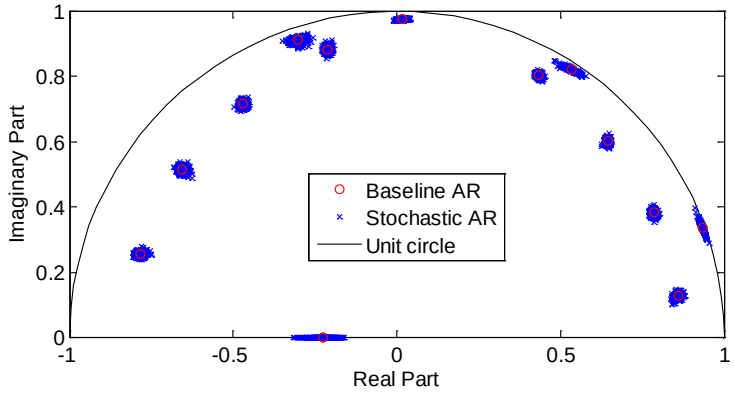

(b)

Figure 7: Analysis for degree of freedom 2. (a) Power spectral densities of the baseline model ("Displacement"), its autoregressive approximation ("Baseline AR"), and the 5th-95th percentile of the band of uncertainty of the stochastic model (in green). (b) Location of poles of the baseline and stochastic AR models in the complex plane. $\delta = 0.1$.

4.3 Vector Case – Buffeting of the F-15

Buffeting is an aerodynamic event which corresponds to the appearance of a massively detached flow, typically occurring at high angles of attack, and leads to randomly time varying pressures and loads on the aircraft. Buffeting can lead to severe vibration problems and has been of concern for the F-15 aircraft. The prediction of the random buffeting loads can be achieved by Computational Fluid Dynamics (CFD) codes, see [14], but typically involves a series of assumptions, e.g., simplified aero-structure interaction or rigid aircraft, specified turbulence model, specified upstream turbulence level, the effects of which on this very complex flow, see Fig. 8, are not currently well understood. It is thus appropriate to assume that the information transmitted to the structural dynamicist, i.e., the spectral matrix of the modal forces on the aircraft, is subject to uncertainty. Another source of uncertainty which may also be present relates to differences in flight conditions used in the computations and experienced

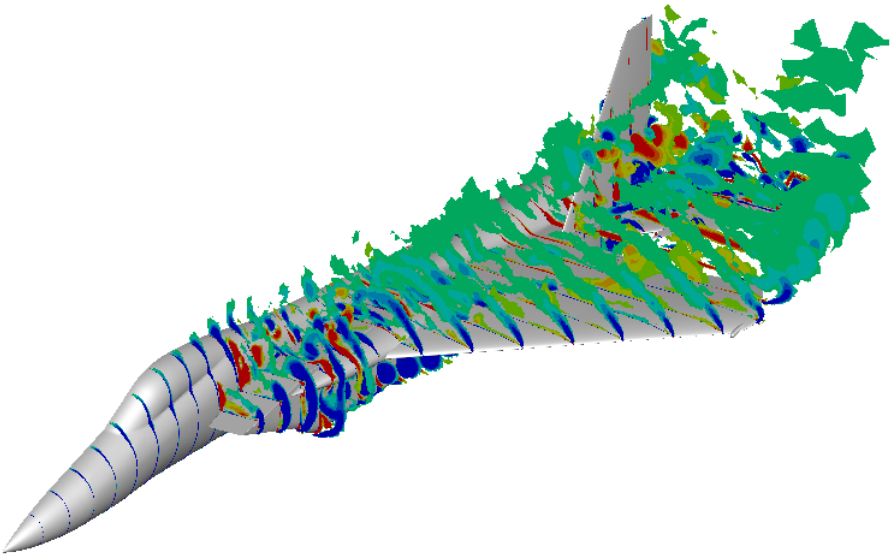

Figure 8: Snapshot of vorticity on the F-15 at angle of attack α= 22.5 deg, half-model shown.

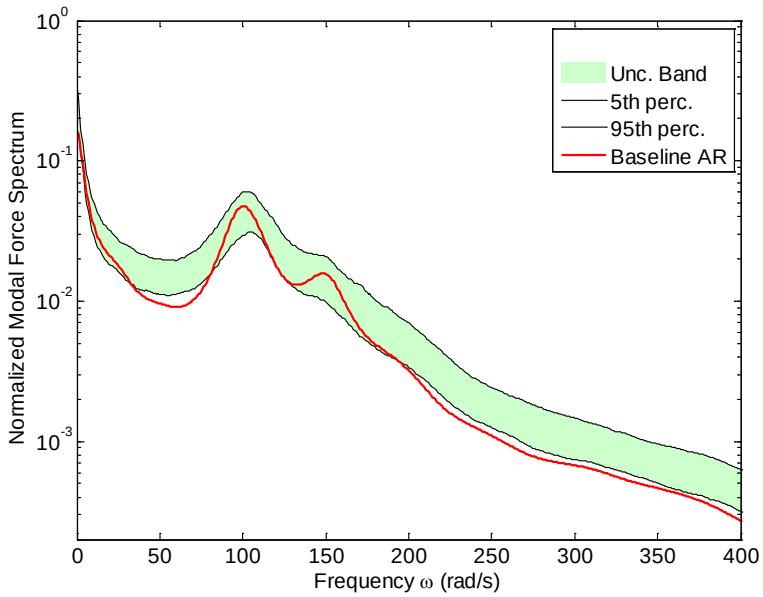

Figure 9: Power spectral density of the modal force of mode 10 induced by the buffet loads, baseline model and 5th-95th uncertainty band shown in green (α = 22.5 deg).

in actual flights. Specifically, the computations are typically performed under assumed constant flight conditions (angle of attack, speed, altitude) but the aircraft is likely to experience time varying (possibly rapidly) flight conditions.

Notwithstanding the possible discrepancies between predictions and flight measurements, it is desired to carry forward the predictions to the estimation of the structural response and potentially fatigue life. The approach proposed here is thus to introduce uncertainty on the power spectral matrix of the modal forces on the structure and to propagate it to the desired response measures – typically in a Monte Carlo format.

The structural model retained for the F-15 included 38 of the first 80 modes and time histories of their modal forces were obtained from the CFD code (FUN3D with DES option) as described in [14]. After removal of the transient, these 38 time histories were modeled as in Eq. (1) with an order m = 11 using a modified version of the Matalb codes of [15]. Shown in

Figs. 9-12 are the auto spectra of two of these modal forces as well as the real and imaginary part of their cross spectrum. Since the aircraft was considered to be a linear structure, the power spectral matrix of the 38 modal coordinates could then be obtained (see [14] for discussion) and from it the power spectral density of any specified response could be derived. Of particular interest here is the power spectral density of the acceleration at the aft end of the tip pod of the left vertical tail, shown on Fig. 13.

Accounting for the stated uncertainties was achieved by independently randomizing the reflection coefficient matrices of the 38 modal forces as described above. An overall uncertainty level of $\delta = 0.3$ was assumed to exemplify the process. Then, shown in Figs 9-13 are the 5th-95th percentiles band of uncertainty on the spectra (as shown by the green band) of the selected modal forces and on the acceleration at the aft end of the tip pod of the left vertical tail.

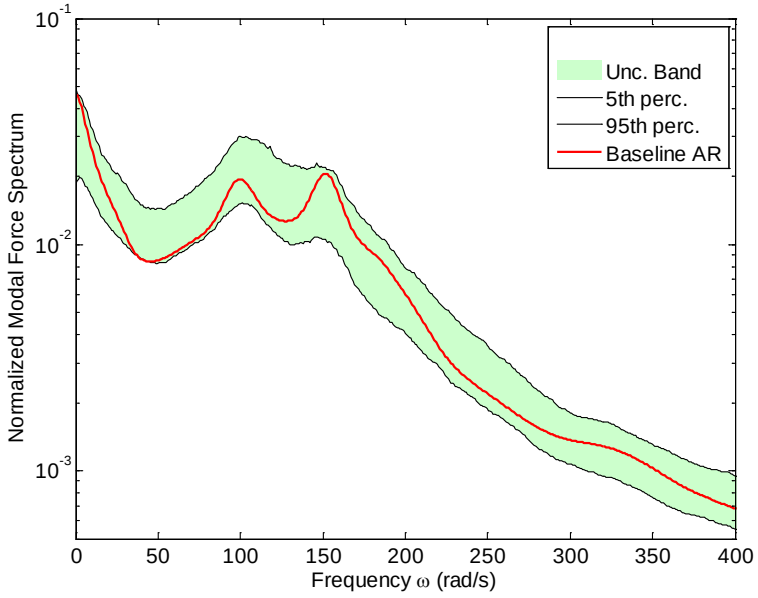

Figure 10: Power spectral density of the modal force of mode 65 induced by the buffet loads, baseline model and 5th-95th uncertainty band shown in green ($\alpha = 22.5$ deg).

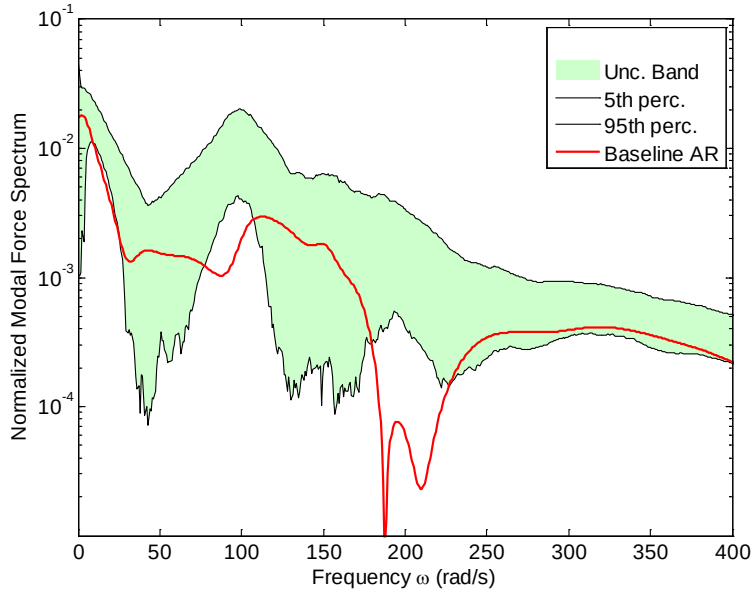

Figure 11: Real part of the cross power spectral density of the modal forces of modes 10 and 65 induced by the buffet loads, baseline model and 5th-95th uncertainty band shown in green ($\alpha = 22.5$ deg).

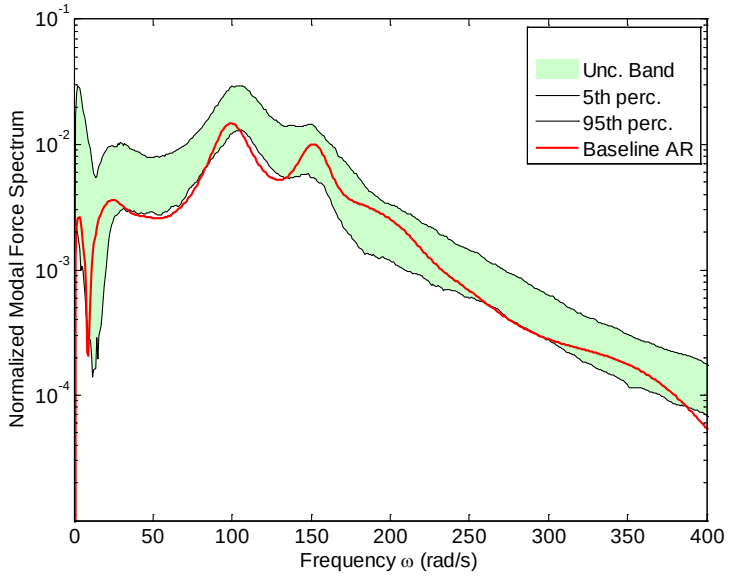

Figure 12: Imaginary part of the cross power spectral density of the modal forces of modes 10 and 65 induced by the buffet loads, baseline model and 5th-95th uncertainty band shown in green (α = 22.5 deg).

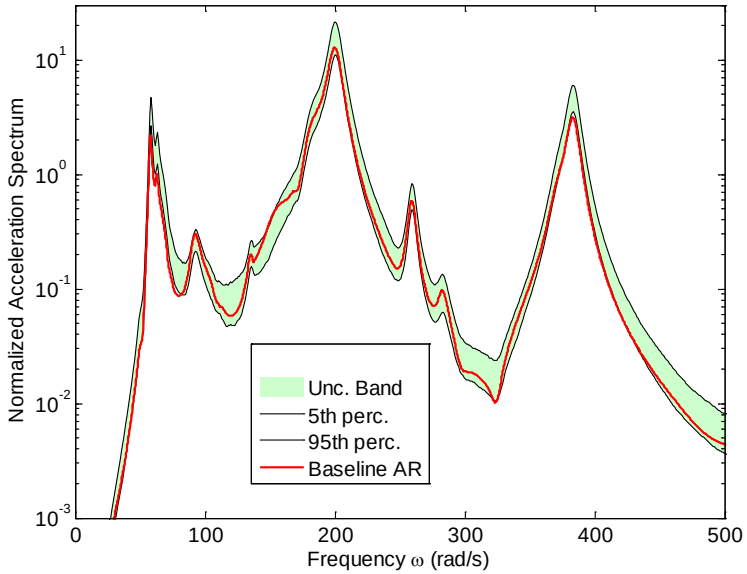

Figure 13: Power spectral density of the acceleration at the aft end of the tip pod of the left vertical tail induced by the buffet loads, baseline model and 5th-95th uncertainty band shown in green (α = 22.5 deg).

4.4 Scalar Case – Model Identification from Data

The last application considered here focuses on the assessment of the proposed model to represent given samples of an uncertain power spectral density. To this end, the 4 degree of freedom system discussed above was randomized, i.e., its mass, stiffness, and damping matrices were simulated (as symmetric positive definite matrices) according to the maximum entropy-based nonparametric method as independent matrices with δ = 0.04 for all three. For this stochastic dynamic system, samples of the power spectral densities of degrees of freedom 1 and 2 were generated and the corresponding uncertainty bands associated with their 5th and 95th percentiles were determined.

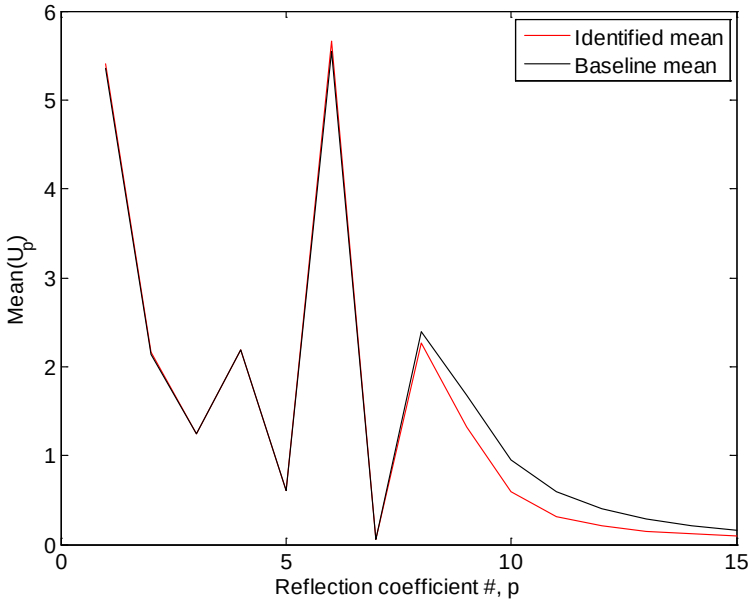

Figure 14: Baseline and identified mean values of the random variables U_p for the 15 reflection coefficients, degree of freedom 1 data.

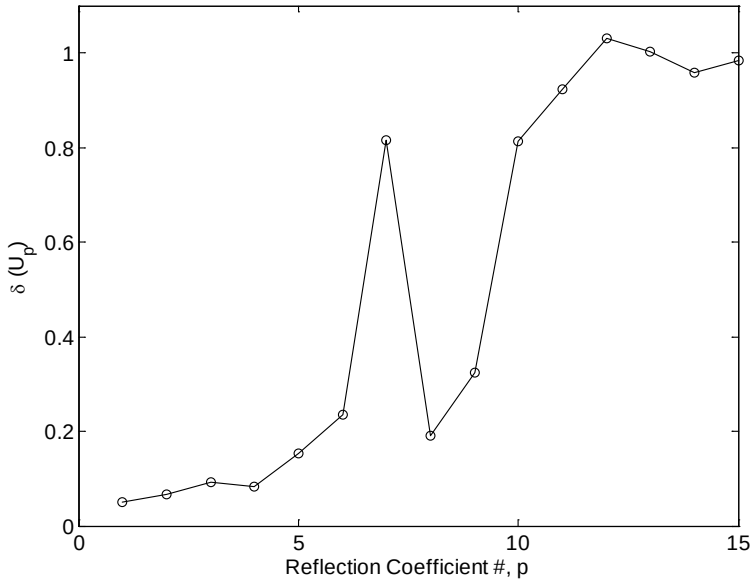

Figure 15: Identified δ values of the random variables U_p for the 15 reflection coefficients, degree of freedom 1 data.

The objective of this section was then to assess the applicability of the stochastic AR model developed in this paper to this data and to compare the autoregressive-based uncertainty bands to the ones derived directly from the stochastic dynamic system. To perform this assessment most cleanly, a large number of samples, 300, of the power spectral densities were generated as to minimize the uncertainty associated with small sample size identification. Autoregressive approximations of each of these 300 power spectral densities were obtained, with orders 15 and 25 for degrees of freedom 1 and 2 as previously justified. The corresponding samples of the reflection coefficients and of the parameters $\hat{B}_0$ were then obtained. Next, the maximum likelihood approach was used to identify the hyperparameters of the model of Eqs

(47) and (48), i.e., the values $\hat{\bar{B}}_0$ and $\bar{U}_p$, p = 0, 1, ..., m-1, and the corresponding δ values of each of these random variables. This identification was carried out for each parameter (reflection coefficient and/or parameter $\hat{B}_0$) independently of each other consistently with their assumed independence in the stochastic autoregressive model.

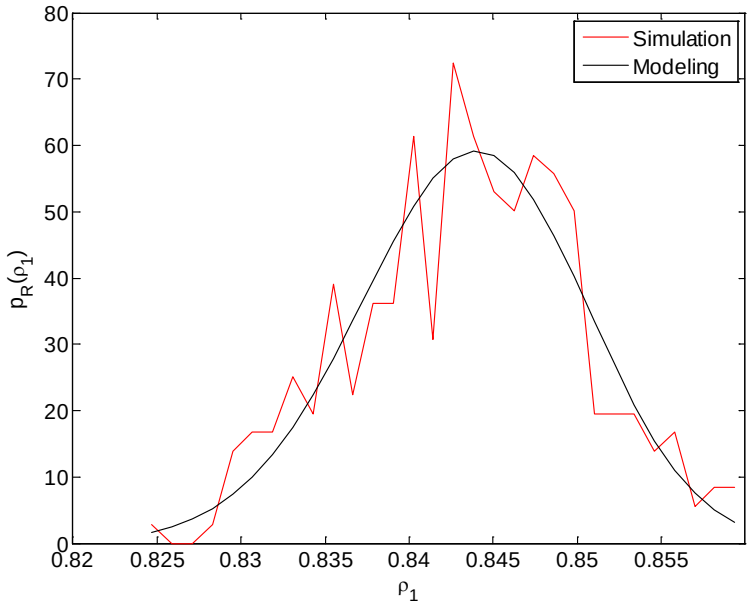

Figure 16: Probability density function of the reflection coefficient #1 estimated from data and model of Eq. (48), degree of freedom 1 data.

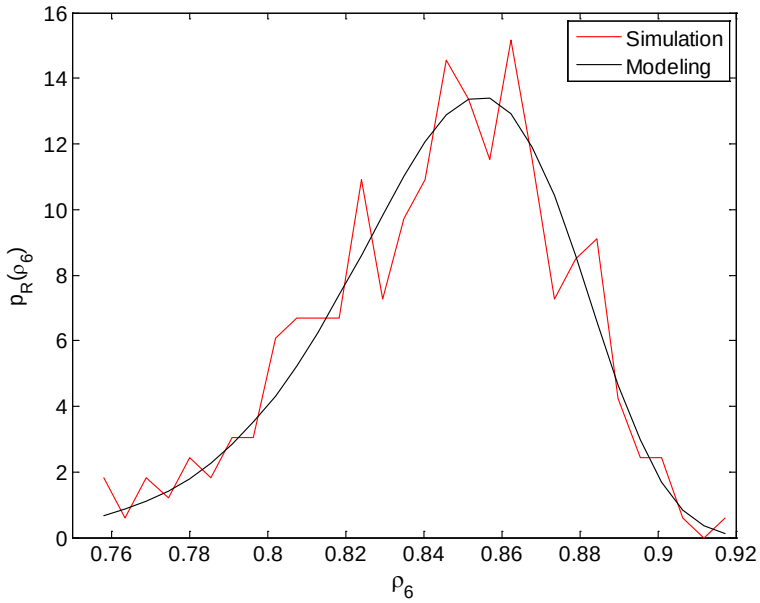

Figure 17: Probability density function of the reflection coefficient #6 estimated from data and model of Eq. (48), degree of freedom 1 data.

Shown in Figs 14 and 15 are the identified values of $\bar{U}_p$ and the corresponding δ values for degree of freedom 1 data. Also shown in Fig. 14 are the values of $\bar{U}_p$ obtained deterministically from the mean autoregressive model obtained earlier. Clearly, the match is very good for most of the reflection coefficients. A more detailed assessment can be drawn from com-

parisons of the probability density functions of the reflections coefficients and shown in Figs 16-19 is a representative set of such plots. Two distinct situations were observed depending on the magnitude of the reflection coefficients. For those with large means, e.g. see Figs 16-18, the probability density function of the reflection coefficient is well to very well matched by the model of Eq. (48). A similar conclusion was drawn in regards to the parameter $\hat{B}_0$, see Fig. 20.

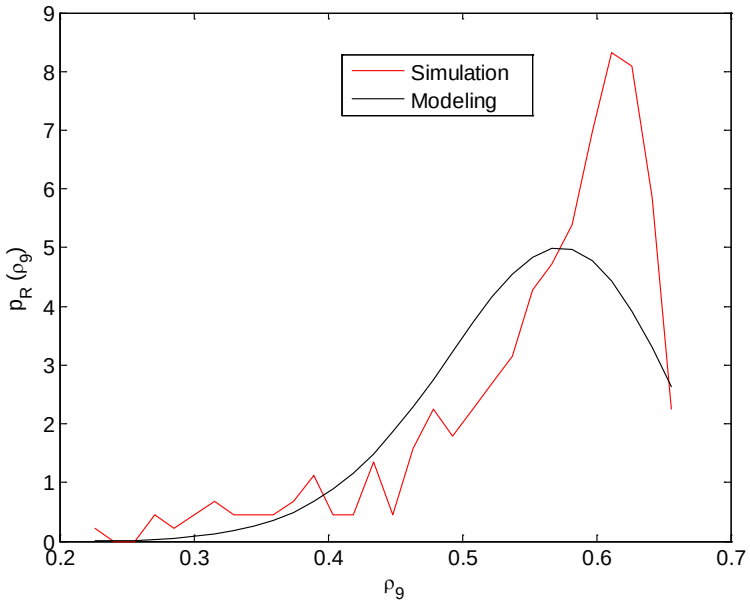

Figure 18: Probability density function of the reflection coefficient #9 estimated from data and model of Eq. (48), degree of freedom 1 data.

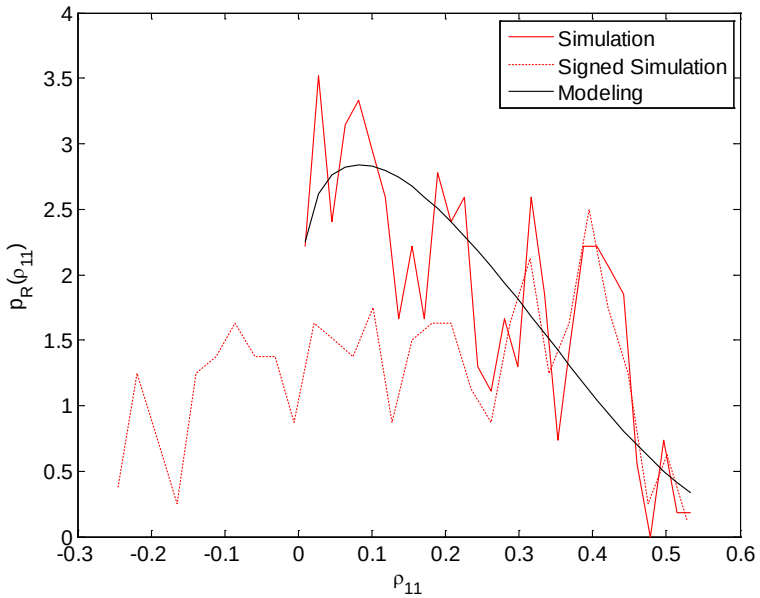

Figure 19: Probability density function of the reflection coefficient #11 estimated from data and model of Eq. (48), degree of freedom 1 data.

The reflection coefficients exhibiting a small mean are typically associated with a very large δ value as can be concluded from Figs 14 and 15. This situation results in fact from sign changes of the reflection coefficient, as seen in Fig. 19 for reflection coefficient 11, which are not accounted for in the model of Eq. (48). Given their magnitudes, these reflection coeffi-

cients and their variability are not expected to significantly affect the stochastic autoregressive predictions. This situation is confirmed in Figs. 21 and 22 which show the uncertainty bands predicted from the stochastic autoregressive model with the identified parameters (Fig. 21) and with the identified parameters except for the δ values of the small reflection coefficients (7,9-15) which were set to the smallest δ identified (0.05 for the first reflection coefficient), see Fig. 22. The band is larger in Fig. 21 than in Fig. 22, but only slightly even though there was a dramatic change in the δ values on reflection coefficients 7 and 9-15. Given this small effect, these reflection coefficients will thus be referred to as "secondary".

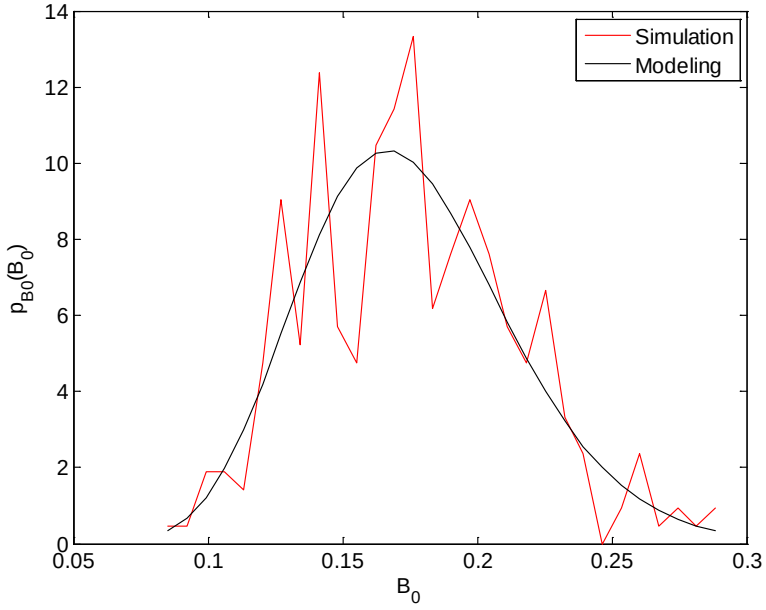

Figure 20: Probability density function of the autoregressive parameter $\hat{B}_0$ estimated from data and model of Eq. (47), degree of freedom 1 data.

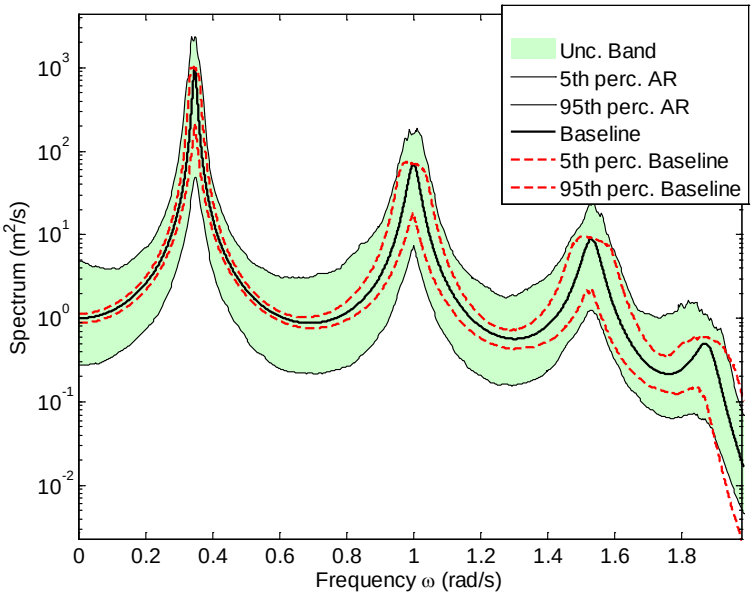

Figure 21: Power spectral densities of the stochastic dynamic systems (baseline curves), mean model and 5th and 95th percentiles, and their identified autoregressive stochastic model counterparts (AR curves and green band). δ values of secondary reflection coefficients as identified, degree of freedom 1 data.

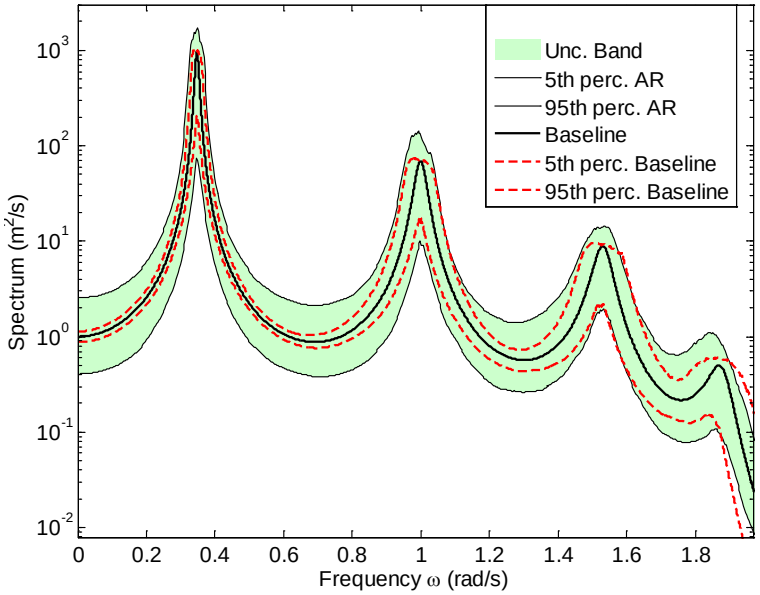

Figure 22: Power spectral densities of the stochastic dynamic systems (baseline curves), mean model and 5th and 95th percentiles, and their identified autoregressive stochastic model counterparts (AR curves and green band). δ values of secondary reflection coefficients set to minimum δ identified, degree of freedom 1 data.

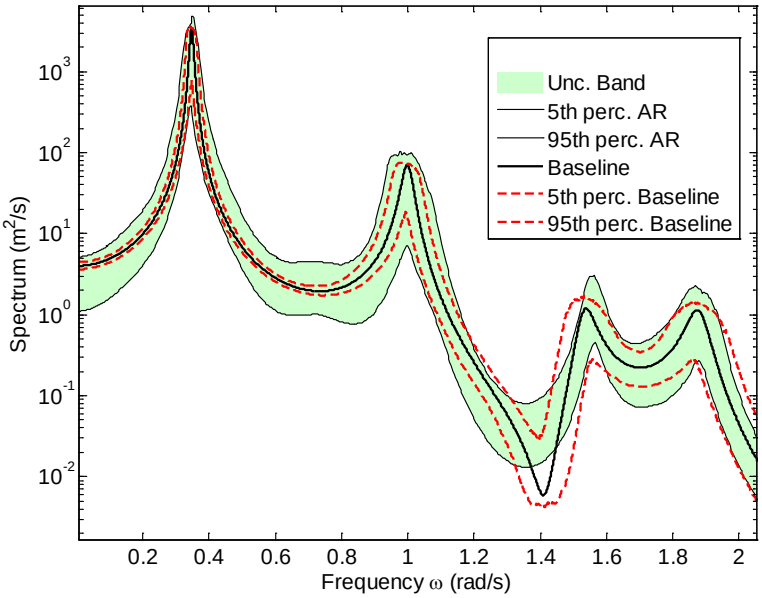

Figure 23: Power spectral densities of the stochastic dynamic systems (baseline curves), mean model and 5th and 95th percentiles, and their identified autoregressive stochastic model counterparts (AR curves and green band). δ values of secondary reflection coefficients set to minimum δ identified, degree of freedom 2 data.

In summary, it is found that the stochastic modeling of the "primary" reflection coefficients (those with large mean values and strongly affecting the power spectral density predictions) and the autoregressive parameters $\hat{B}_0$ by the models of Eqs (47) and (48) is very good to excellent. The secondary reflection coefficients are not as well modeled, with their δ values typically very large, but this only has a small effect on the predicted uncertainty bands.

It remains to assess how well the uncertainty bands predicted from the stochastic autoregressive model matches the ones derived directly from the stochastic dynamic system, see Fig. 22 and Fig. 23 for the degree of freedom 2. It is seen from these figures that the uncertainty bands from the stochastic AR model match appropriately well their dynamic system counterparts in the critical zones, i.e., near the peaks. The bands are otherwise wider, and thus typically on the safe side, in the smaller energy regions.

5 SUMMARY

The focus of this investigation was on the formulation and assessment of a stochastic modeling strategy of uncertainty on the specification of the power spectral density of scalar stationary processes and on the spectral matrices of vector ones. This stochastic model is based on an autoregressive-based parameterization of the specified baseline power spectral density/matrix and of its random samples. To insure stability of these autoregressive models, their parametrization was performed in terms of their reflection coefficients which lie (or their eigenvalues in the vector process case) in the domain [0,1). Maximum entropy concepts were then employed to formulate the distribution of the reflection coefficients in both scalar and vector process case leading to a small set of hyperparameters of the uncertain model. Three examples of validation were presented to clarify the properties of the modeling. The procedure was found straightforward of application on examples ranging in complexity from a 4th order scalar model to an 11th order vector case involving 38 components. It was further found that the uncertainty affects all aspects of the power spectral density/matrix: magnitude, peak location, location of poles and permits the convenient determination of a percentile-based band of uncertainty on the power spectral densities. A fourth example was considered that demonstrated the successful application of the approach to model existing samples of an uncertain power spectral density.

ACKNOWLEDGEMENTS

The financial support of this work by the Air Force STTR Phase II contract FA9550-13-C-0022 with Dr. Michael Kendra as Technical Monitor is gratefully acknowledged.

REFERENCES

[1] S.L. Marple, *Digital Spectral Analysis With Applications*. Prentice Hall, 1987.

[2] M.P. Mignolet, P.D. Spanos, Autoregressive spectral modeling: difficulties and remedies. *International Journal of Non-Linear Mechanics*, **26**, 911-930, 1991.

[3] E.R. Beadle, P.M. Djuric, Uniform random parameter generation of stable minimum-phase real ARMA (p,q) processes. *IEEE Signal Processing Letters*, **4**, 259-261, 1997.

[4] M. Rahiala, Random coefficient autoregressive models for longitudinal data. *Biometrika*, **86**, 718-722, 1999.

[5] P. Shcherbakov, F. Dabbene, On the generation of random stable polynomials. *European Journal of Control*, **2**, 145–159, 2011.

[6] C.T. Ng, H. Joe, Generating random AR(p) and MA(q) Toeplitz correlation matrices. *Journal of Multivariate Analysis*, **101**, 1532-1545, 2010.

[7] R.A. Wiggins, E.A. Robinson, Recursive solution to the multichannel filtering problem. *Journal of Geophysical Research*, **70**, 1885-1891, 1965.

[8] M. Morf, A. Vieira, T. Kailath, Covariance characterization by partial autocorrelation matrices. *The Annals of Statistics*, **6**, 643-648, 1978.

[9] C. Soize, A nonparametric model of random uncertainties on reduced matrix model in structural dynamics. *Probabilistic Engineering Mechanics*, **15**, 277-294, 2000.

[10] C. Soize, *Stochastic Models of Uncertainties in Computational Mechanics*. American Society of Civil Engineers (ASCE), 2012.

[11] S. Das, R. Ghanem, A bounded random matrix approach for stochastic upscaling. *Multiscale Modeling and Simulation*, **8**, 296-325, 2009.

[12] J. Guilleminot, A. Noshadravan, C. Soize, C., R.G. Ghanem, A probabilistic model for bounded elasticity tensor random fields with application to polycrystalline microstructures. *Computer Methods in Applied Mechanics and Engineering*, **200**, 1637–1648, 2011.

[13] M.P. Mignolet, C. Soize, Nonparametric stochastic modeling of linear systems with prescribed variance of several natural frequencies. *Probabilistic Engineering Mechanics*, **23**, 267-278, 2008.

[14] S. Yang, P.C. Chen, X.Q. Wang, M.P. Mignolet, D.M. Pitt, J. Loyet, Prediction of F-15 buffet loads using a computational fluid dynamics approach. *Journal of Aircraft*, Submitted for Publication.

[15] H. Hytti, R. Takalo, H. Ihalainen, Matlab Functions for MAR Modeling, Downloaded from http://www.mit.tut.fi/staff/hytti/MAR_modelling.html.